

# Torsional oscillation of carbon nanotubes driven by electron spins

Koji Yamada,<sup>1</sup> Wataru Izumida,<sup>2</sup> Mamoru Matsuo,<sup>3,4,5,6</sup> and Takeo Kato<sup>1</sup>

<sup>1</sup>*Institute for Solid State Physics, University of Tokyo, Kashiwa 277-8581, Japan*

<sup>2</sup>*Department of Physics, Tohoku University, Sendai 980-8578, Japan*

<sup>3</sup>*Kavli Institute for Theoretical Sciences, University of Chinese Academy of Sciences, Beijing, 100190, China.*

<sup>4</sup>*CAS Center for Excellence in Topological Quantum Computation,  
University of Chinese Academy of Sciences, Beijing 100190, China*

<sup>5</sup>*Advanced Science Research Center, Japan Atomic Energy Agency, Tokai, 319-1195, Japan*

<sup>6</sup>*RIKEN Center for Emergent Matter Science (CEMS), Wako, Saitama 351-0198, Japan*

(Dated: March 16, 2026)

We theoretically investigate the current-induced excitation of torsional vibrations in a suspended carbon nanotube (CNT) quantum dot. By considering a CNT clamped between half-metallic ferromagnetic electrodes with an antiparallel magnetization configuration, we demonstrate that the spin-rotation coupling enables the transfer of angular momentum from electron spins to the mechanical torsional mode under a constant source-drain voltage. Using a master-equation approach to analyze the coupled dynamics of the dot levels and a quantized torsional oscillator, we evaluate the steady-state current and phonon distribution. We find that when the Zeeman splitting matches the torsional phonon energy, the system exhibits a sharp resonant behavior in the current, accompanied by a significant increase in the phonon population. Our estimates for realistic device parameters indicate that this spin-driven mechanism can drive CNT torsional vibrations with detectable amplitudes. This work provides a theoretical basis for current-controlled actuation of nanoelectromechanical systems via the spin angular momentum of electrons.

## I. INTRODUCTION

Carbon nanotubes (CNTs) form a standard platform for nanoelectromechanical systems (NEMS) because a single suspended tube combines a small mass with a large stiffness and can reach high resonance frequencies [1–4]. While carbon nanotubes played a central role in early studies of NEMS, recent advances have extended NEMS research to a variety of nanomaterials [5]. Beyond flexural motion, torsional degrees of freedom of CNT devices have also been resolved, including torsion springs and torsional resonators [6–8]. A suspended CNT simultaneously acts as a quantum dot, so that electronic transport and a selected mechanical mode can be treated within a single nanoscale device [9–14]. This setting invites actuation schemes in which the mechanical variable is driven by a microscopic channel of angular-momentum transfer rather than by an electrostatic force.

Electrical actuation in NEMS is often based on capacitive forces and therefore couples most directly to displacement [15]. This coupling fits naturally with flexural modes, where the generalized force is a transverse force. The torsional mode, by contrast, couples to a torque about the tube axis. Although a controlled torque can be generated using torsional nanomechanical devices [6–8], this approach constrains device geometry and electrode design. A torque-based drive is nonetheless of interest because torsional motion probes mechanical angular momentum directly and provides a route to couple nanomechanics to the internal angular momentum carried by electrons.

A microscopic source of torque is provided by the conversion between spin angular momentum and mechanical rotation. The classical gyromagnetic effects, associ-

ated with the Barnett and Einstein–de Haas effects [16–19], express the exchange of angular momentum between magnetization and rotation. The gyromagnetic effects have attracted renewed attention in the 21st century in the context of spin current induced by inhomogeneities of the angular velocity [20–31]. They have also been utilized for mechanical torsion generation using electron spin relaxation on nanoscale objects [32–36]. In a quantum description, the coupling between a rotating frame and an electron spin is given by the spin-rotation coupling (SRC) [37, 38]

$$\hat{H}_{\text{SR}} = -\boldsymbol{\omega} \cdot \hat{\boldsymbol{S}}, \quad (1)$$

where  $\boldsymbol{\omega}$  is the angular velocity and  $\hat{\boldsymbol{S}}$  is the spin operator. Equation (1) implies that a spin flip can act as a torque impulse on a mechanical coordinate that carries angular momentum. In CNTs, where twisting motion is well defined and can be quantized [39], SRC-mediated spin–phonon conversion has been discussed in several contexts [40].

A recent example of SRC-based actuation is the Einstein–de Haas nanorotor proposed by Izumida et al. [41]. In that setup, a CNT quantum dot is embedded between ferromagnetic electrodes with antiparallel magnetizations. Under steady bias, a current requires spin-flip processes on the dot, and each spin flip transfers angular momentum to the mechanical rotation through Eq. (1). Ref. [41] demonstrated continuous rigid-body rotation induced by this angular momentum transfer and discussed the efficiency of conversion from electron spins to rotation of the CNT.

The present work considers a complementary regime in which the mechanical degree of freedom is not rigid-body rotation but the fundamental torsional mode of a

suspended CNT clamped between two electrodes. The clamped geometry removes the need to engineer a bearing for a freely rotating shaft while still allowing a well-defined mechanical angular velocity associated with torsional vibration. The device is again operated in a spin-selective transport configuration using ferromagnetic electrodes with antiparallel magnetizations. For simplicity, we consider fully spin-polarized ferromagnetic (half-metallic) electrodes in the main calculation, while partially spin-polarized electrodes are discussed in Sec. V A. A steady current is then limited by the spin valve effect, and transport proceeds through spin flips on the dot. Because SRC couples each spin-flip event to the exchange of mechanical angular momentum, electron transport can pump the torsional oscillator by creating (and absorbing) torsional phonons. The pumping is most efficient when the Zeeman splitting  $h$  is tuned close to the torsional phonon energy,  $h \simeq \hbar\omega_0$ , within the linewidth of the mechanical resonance, where  $\omega_0$  is the eigenfrequency of the fundamental torsional mode. This produces a sharp transport signature: the steady-state current exhibits a ridge along the resonance line, accompanied by a nonequilibrium increase in the phonon population.

We analyze this mechanism using a master equation approach for the coupled dynamics of the dot and a quantized torsional mode. The calculation yields the steady-state phonon distribution and the current as functions of bias, magnetic field, temperature, and the relaxation rate of the torsional mode. For parameter values consistent with suspended CNT devices, the resulting torsional angle at the center of the tube reaches an angle of order one degree in the driven steady state. The theory thus provides a route to torque actuation of CNT torsional modes by spin angular momentum, distinct from force-based electrical drives that mainly address flexural motion.

The remainder of the paper is organized as follows. Section II introduces the model Hamiltonian and the SRC-mediated spin-phonon coupling for a clamped CNT torsional mode. Section III presents the master equation and the transition rates. Section IV discusses the steady-state current and the phonon distribution, including the resonance and the dependence on relaxation and temperature. Section V comments on the effects of realistic ferromagnetic electrodes with finite spin polarization, as well as extensions to realistic CNT spectra with valley degrees of freedom and spin-orbit interaction. Section VI summarizes the results.

## II. MODEL

We consider a suspended single-wall CNT of length  $L$ , whose ends are rigidly clamped by ferromagnetic electrodes, as illustrated in Fig. 1. The left and right electrodes are assumed to be half-metallic, magnetized along the  $+z$  and  $-z$  directions, respectively. A static magnetic

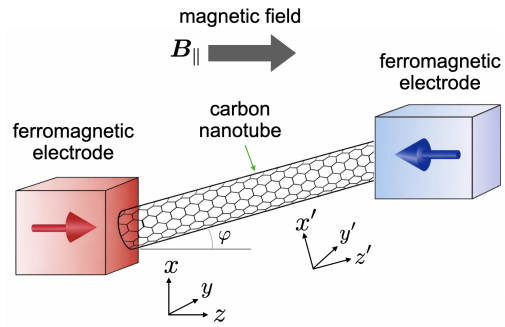


FIG. 1. Schematic illustration of the model: A suspended CNT of length  $L$  is connected to half-metallic ferromagnetic electrodes magnetized along opposite directions.

field  $\mathbf{B} \parallel \hat{z}$  is applied. The axis of the CNT is tilted by an angle  $\varphi$  with respect to the magnetic-field direction. The system Hamiltonian is given by

$$H = H_{\text{dot}} + H_{\text{lead}} + H_{\text{lead-dot}} + H_{\text{ph}} + H_{\text{env}} + H_{\text{ph-env}} + H_{\text{SR}}, \quad (2)$$

where  $H_{\text{dot}}$ ,  $H_{\text{lead}}$ , and  $H_{\text{lead-dot}}$  describe the CNT quantum dot, the electronic leads, and the lead-dot tunneling interaction, respectively.  $H_{\text{ph}}$  represents the phonons of the torsional mode, which are coupled to the thermal phonon environment  $H_{\text{env}}$  via the interaction term  $H_{\text{ph-env}}$ . Finally,  $H_{\text{SR}}$  denotes the spin-rotation interaction originating from the gyromagnetic effect. In the subsequent subsections, we present an explicit form of each Hamiltonian.

### A. Electron systems

At cryogenic temperatures, the CNT can be regarded as a quantum dot with discrete electronic levels. For simplicity, we consider a single-level quantum dot, whose Hamiltonian is given by

$$H_{\text{dot}} = \left( \epsilon_d + \frac{h}{2} \right) d_{\uparrow}^{\dagger} d_{\uparrow} + \left( \epsilon_d - \frac{h}{2} \right) d_{\downarrow}^{\dagger} d_{\downarrow} + U n_{\uparrow} n_{\downarrow}, \quad (3)$$

where  $d_{\sigma}$  is an annihilation operator for electrons with spin  $\sigma$  ( $\sigma = \uparrow, \downarrow$ ),  $n_{\sigma} = d_{\sigma}^{\dagger} d_{\sigma}$  is an electron number operator,  $\epsilon_d$  is the single-particle energy level of the quantum dot, and  $h = g\mu_B B$  ( $g$ : the  $g$ -factor,  $\mu_B$ : the Bohr magneton) denotes the Zeeman energy induced by the external magnetic field. We neglect the valley degree of freedom in the CNT (see Sec. V B for a discussion of the spin-orbit interaction). Following the standard convention in quantum-dot systems, electron spins parallel or antiparallel to the magnetic field are denoted as  $\uparrow$  and  $\downarrow$ , respectively. The Coulomb interaction  $U$  is assumed to be sufficiently large that only the unoccupied state (denoted by 0) and the one-electron occupied states (denoted by  $\uparrow$  and  $\downarrow$ ) are relevant. The energies of these states are

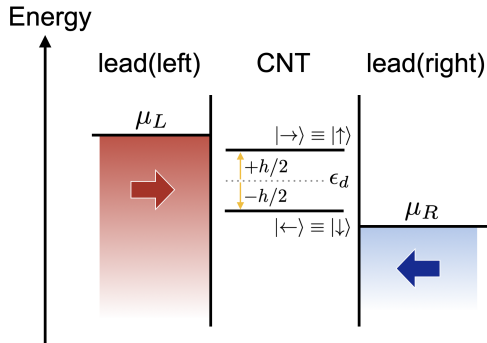


FIG. 2. Energy-level diagram of the CNT quantum dot.

given by  $\epsilon_0 = 0$ ,  $\epsilon_{\uparrow} = \epsilon_d + \hbar/2$ , and  $\epsilon_{\downarrow} = \epsilon_d - \hbar/2$ . The energy level diagram of the quantum dot is shown in Fig. 2.

The coupling between the CNT and the completely spin-polarized (half-metallic) leads is described by the tunneling Hamiltonian

$$H_{\text{lead}} = \sum_{\mathbf{k}} (\epsilon_{\mathbf{k}} - \mu_L) c_{L\mathbf{k}\uparrow}^{\dagger} c_{L\mathbf{k}\uparrow} + \sum_{\mathbf{k}} (\epsilon_{\mathbf{k}} - \mu_R) c_{R\mathbf{k}\downarrow}^{\dagger} c_{R\mathbf{k}\downarrow}, \quad (4)$$

$$H_{\text{lead-dot}} = \sum_{\mathbf{k}} (\Delta_L d_{\uparrow}^{\dagger} c_{L\mathbf{k}\uparrow} + \Delta_R d_{\downarrow}^{\dagger} c_{R\mathbf{k}\downarrow} + \text{H.c.}), \quad (5)$$

where  $c_{L\mathbf{k}\uparrow}$  and  $c_{R\mathbf{k}\downarrow}$  denote annihilation operators for electrons with wave vector  $\mathbf{k}$  in the two electrodes,  $\mu_L$  and  $\mu_R$  are the chemical potentials of the left and right leads, and  $\Delta_L$  and  $\Delta_R$  are tunneling amplitudes.

### B. Torsional vibration

We first consider the torsional (twisting) vibration modes of the CNT within the classical continuum model. Due to its cylindrical symmetry, the vibration mode is described by a twist angle  $\theta(z', t)$ , where a new coordinate  $(x', y', z')$  is introduced so that the  $z'$  axis is aligned with the axis of the CNT. The restoring torque per unit length resulting from shear deformation is given by

$$\tau(z') = GR^2S \frac{\partial^2 \theta}{\partial z'^2}, \quad (6)$$

where  $R$  is the CNT radius,  $S = 2\pi R d$  is a cross-section area of the CNT,  $d$  is the wall thickness, and  $G$  is the shear modulus. Assuming a hollow cylinder and linearized dynamics, the equation of motion reads

$$\frac{\partial^2 \theta}{\partial t^2} = c^2 \frac{\partial^2 \theta}{\partial z'^2}, \quad c = \sqrt{\frac{GS}{\rho}}, \quad (7)$$

where  $\rho$  is the mass density of the CNT per unit length. For a CNT of length  $L$ , clamped boundary conditions

$\theta(0, t) = \theta(L, t) = 0$  lead to quantized normal modes of the form

$$\theta(z', t) = \sum_{n=1}^{\infty} \sqrt{\frac{2}{L}} \sin\left(\frac{n\pi z'}{L}\right) \theta_n(t). \quad (8)$$

In the following, we consider only the fundamental mode ( $n = 1$ ) and denote its angular frequency as  $\omega_0 = \pi c/L$ .

Next, we consider the quantization of the fundamental torsional mode. The phonon Hamiltonian reads

$$H_{\text{ph}} = \hbar\omega_0 \left( a^{\dagger} a + \frac{1}{2} \right), \quad (9)$$

where  $a$  and  $a^{\dagger}$  are bosonic annihilation and creation operators defined as

$$\hat{a} = \sqrt{\frac{\rho R^2 \omega_0}{2\hbar}} \left[ \hat{\theta} + i \frac{\hat{\pi}}{\rho R^2 \omega_0} \right], \quad (10)$$

$$\hat{a}^{\dagger} = \sqrt{\frac{\rho R^2 \omega_0}{2\hbar}} \left[ \hat{\theta} - i \frac{\hat{\pi}}{\rho R^2 \omega_0} \right]. \quad (11)$$

Here,  $\hat{\theta}$  ( $= \hat{\theta}_1$ ) is the operator representing the amplitude of the fundamental torsional mode, and  $\hat{\pi}$  is an operator canonically conjugate to  $\hat{\theta}$ , which satisfies  $[\hat{\theta}, \hat{\pi}] = i\hbar$ . For detailed derivation, see Appendix A. From Eq. (9), the time evolution of the twist angle operator  $\hat{\theta}(z', t)$  is given by

$$\hat{\theta}(z', t) \simeq \sqrt{\frac{2}{L}} \sin\left(\frac{\pi z'}{L}\right) \hat{\theta}(t), \quad (12)$$

$$\hat{\theta}(t) = \sqrt{\frac{\hbar}{2\rho R^2 \omega_0}} (\hat{a} e^{-i\omega_0 t} + \hat{a}^{\dagger} e^{i\omega_0 t}). \quad (13)$$

To describe the damping of the torsional mode, we consider energy dissipation into a phonon environment associated with the junctions. We model this damping with an environment described by the Hamiltonian

$$H_{\text{env}} = \sum_{\mathbf{q}} \hbar\omega_{\mathbf{q}} \left( b_{\mathbf{q}}^{\dagger} b_{\mathbf{q}} + \frac{1}{2} \right), \quad (14)$$

$$H_{\text{ph-env}} = \sum_{\mathbf{q}} \kappa (a^{\dagger} b_{\mathbf{q}} + a b_{\mathbf{q}}^{\dagger}), \quad (15)$$

where  $b_{\mathbf{q}}$  and  $b_{\mathbf{q}}^{\dagger}$  are annihilation and creation operators for the bath phonon modes with wave vector  $\mathbf{q}$ , respectively, and  $\kappa$  denotes the coupling constant between the torsional mode and the environmental phonon modes.

### C. Spin-rotation coupling

The key mechanism for the conversion between electron spins and torsional vibrations (phonons) is the gyromagnetic effect, which is the conversion of angular momentum between spin and mechanical rotation. This

angular-momentum conversion is expressed by the spin-rotation coupling,  $-\boldsymbol{\omega} \cdot \hat{\mathbf{S}}$ , where  $\boldsymbol{\omega}$  is the angular velocity of the rigid-body rotation and  $\hat{\mathbf{S}}$  is the total spin in the target material. This spin-rotation coupling can be extended to local mechanical rotation expressed by  $\boldsymbol{\omega}(\mathbf{r}) = \hat{\boldsymbol{\Omega}}(\mathbf{r})/2$ , where  $\hat{\boldsymbol{\Omega}}(\mathbf{r})$  is a vorticity defined by

$$\hat{\boldsymbol{\Omega}}(\mathbf{r}) = \nabla \times \hat{\mathbf{v}}(\mathbf{r}). \quad (16)$$

Here,  $\mathbf{r} = x'\mathbf{e}_{x'} + y'\mathbf{e}_{y'} + z'\mathbf{e}_{z'}$  is the position on the CNT, and  $\hat{\mathbf{v}}(\mathbf{r})$  is the velocity field defined by

$$\hat{\mathbf{v}}(\mathbf{r}) = R \left. \frac{\partial \hat{\theta}(z', t)}{\partial t} \right|_{t=0} \mathbf{e}_\perp, \quad (17)$$

with a unit tangent vector  $\mathbf{e}_\perp$  of the CNT. Substituting Eqs. (12) and (13) into this expression, the vorticity is rewritten as

$$\hat{\boldsymbol{\Omega}}(\mathbf{r}) = \frac{i}{2} \sqrt{\frac{\hbar\omega_0}{L\rho R^2}} (\hat{a} - \hat{a}^\dagger) \begin{pmatrix} (\pi x'/L) \cos(\pi z'/L) \\ (\pi y'/L) \cos(\pi z'/L) \\ -2 \sin(\pi z'/L) \end{pmatrix}. \quad (18)$$

The spin-rotation coupling in the CNT is described by the Hamiltonian

$$H_{\text{SR}} = -\frac{Rd}{2} \int_0^L dz' \int_0^{2\pi} d\theta \hat{\boldsymbol{\Omega}}(\mathbf{r}) \cdot \hat{\mathbf{S}}(\mathbf{r}), \quad (19)$$

$$\hat{\mathbf{S}}(\mathbf{r}) = \frac{\hbar}{2} (\hat{\Psi}_\uparrow^\dagger(\mathbf{r}) \hat{\Psi}_\downarrow^\dagger(\mathbf{r})) \boldsymbol{\sigma} \begin{pmatrix} \hat{\Psi}_\uparrow(\mathbf{r}) \\ \hat{\Psi}_\downarrow(\mathbf{r}) \end{pmatrix}, \quad (20)$$

where  $(\theta, z')$  denotes the position on the CNT in the cylindrical coordinate system,  $\hat{\Psi}_\sigma(\mathbf{r})$  is an electron annihilation operator at  $\mathbf{r}$  for spin  $\sigma$ ,  $\hat{\mathbf{S}}(\mathbf{r})$  is the electron spin operator, and  $\boldsymbol{\sigma} = (\sigma_x, \sigma_y, \sigma_z)$  represents the Pauli matrices. By focusing on one eigenstate  $\psi(\mathbf{r})$  in the CNT as a quantum-dot level, the electron field operator is approximated as  $\hat{\Psi}(\mathbf{r}) = \sum_\sigma \psi(\mathbf{r}) d_\sigma$ . For simplicity, we neglect the valley degree of freedom and assume a uniform wavefunction  $\psi(\mathbf{r}) = 1/\sqrt{2\pi R d L}$ . After performing the integral given in Eq. (19) with Eq. (18), the Hamiltonian  $H_{\text{SR}}$  is given by

$$H_{\text{SR}} = \frac{2i}{\pi R} \sqrt{\frac{\hbar\omega_0}{L\rho}} (\hat{a} - \hat{a}^\dagger) \hat{s}_{z'}, \quad (21)$$

where  $\hat{s}_{z'}$  is the  $z'$ -component of the electron spin in the quantum dot ( $\hat{\mathbf{s}} = \hat{s}_{z'} \mathbf{e}_{z'}$ ). The spin-rotation coupling remains only in the  $z'$ -direction, which corresponds to the axis of the CNT. This means that an effective ac magnetic field induced by the CNT torsional modes appears only in the  $z'$  direction. The spin-rotation coupling is rewritten with the spin components in the laboratory coordinates ( $\hat{\mathbf{s}} = \hat{s}_x \mathbf{e}_x + \hat{s}_y \mathbf{e}_y + \hat{s}_z \mathbf{e}_z$ ) as

$$H_{\text{SR}} = \frac{2i}{\pi R} \sqrt{\frac{\hbar\omega_0}{L\rho}} (\hat{a} - \hat{a}^\dagger) \left[ \cos\varphi \hat{s}_z - \frac{\sin\varphi}{2} (\hat{s}_+ + \hat{s}_-) \right], \quad (22)$$

where  $\varphi$  is the tilting angle (see Fig. 1) and the spin operators are related to the creation and annihilation operators of electrons in the quantum dot as  $\hat{s}_z = (\hbar/2)(d_\uparrow^\dagger d_\uparrow - d_\downarrow^\dagger d_\downarrow)$ ,  $\hat{s}_+ = \hbar d_\uparrow^\dagger d_\downarrow$ , and  $\hat{s}_- = (\hat{s}_+)^\dagger$ . The tilting of the CNT axis with respect to the magnetization of the electrodes is required to produce the spin-flipping terms in  $H_{\text{SR}}$ , which enable mutual conversion between the spin angular momentum of electrons and the mechanical angular momentum of the CNT.

### III. FORMULATION

In this work, we calculate transport properties by the method of the master equation. The fundamental torsional mode is regarded as a harmonic oscillator, and its quantum state is denoted with  $m$  ( $= 0, 1, 2, \dots$ ). Combining this with the electronic state in the quantum dot, we label the eigenstates as  $(0, m)$ ,  $(\uparrow, m)$ , and  $(\downarrow, m)$ . In the following, we calculate the transition rates between the states based on Fermi's golden rule using perturbative treatment with respect to  $H_{\text{ph-env}}$ ,  $H_{\text{lead-dot}}$ , and  $H_{\text{SR}}$ .

#### A. Phonon energy relaxation

The relaxation and excitation by the phonon bath are expressed by the transition process induced by  $H_{\text{ph-env}}$ . The relaxation rate from  $(\alpha, m)$  to  $(\alpha, m-1)$ , keeping the electronic state  $\alpha$  ( $= 0, \uparrow, \downarrow$ ) unchanged, is calculated as

$$\Gamma_{(\alpha, m) \rightarrow (\alpha, m-1)} = \frac{2\pi}{\hbar^2} \kappa^2 m \mathcal{D}(\omega_0) [1 + f_{\text{BE}}(\omega_0)], \quad (23)$$

where  $\mathcal{D}(\omega_0)$  denotes the phonon density of states of the bath evaluated at the system frequency  $\omega_0$ ,  $f_{\text{BE}}(\omega) = (e^{\hbar\omega/k_{\text{B}}T} - 1)^{-1}$  is the Bose-Einstein distribution function,  $k_{\text{B}}$  is the Boltzmann constant, and we have assumed that the phonon bath is in thermal equilibrium with the temperature  $T$ . Similarly, the excitation rate from  $|\alpha, m-1\rangle$  to  $|\alpha, m\rangle$  is calculated as

$$\Gamma_{(\alpha, m-1) \rightarrow (\alpha, m)} = \frac{2\pi}{\hbar^2} \kappa^2 m \mathcal{D}(\omega_0) f_{\text{BE}}(\omega_0). \quad (24)$$

In the following, we denote the prefactor as

$$k_{\text{relax}} \equiv \frac{2\pi}{\hbar^2} \kappa^2 \mathcal{D}(\omega_0). \quad (25)$$

At sufficiently low temperatures ( $k_{\text{B}}T \ll \hbar\omega_0$ ),  $k_{\text{relax}}$  corresponds to the mechanical damping rate  $\gamma_{\text{mech}} = \omega_0/Q$ , where  $Q$  is the quality factor of the torsional mode. The realistic value of  $Q$  is expected to range from  $10^2$  to  $10^5$  in experiments at low temperatures, based on experiments for flexural modes [7, 9].

## B. Electron transfer via lead-dot coupling

The electron transfer rates between the CNT and the half-metallic electrodes are calculated from the lead-dot interaction  $H_{\text{lead-dot}}$ . The transition rate for transferring electrons from the left lead to the empty dot is calculated as

$$\Gamma_{(0,m) \rightarrow (\uparrow,m)} = \Gamma_L f_L \left( \epsilon_d + \frac{\hbar}{2} \right), \quad (26)$$

where  $f_L(\epsilon) = (e^{(\epsilon - \mu_L)/k_B T} + 1)^{-1}$  is the Fermi-Dirac distribution of the left lead,  $\Gamma_L = 2\pi \Delta_L^2 D(\epsilon_F)/\hbar$  denotes the tunneling rate, and  $D(\epsilon_F)$  is the density of states at the Fermi energy. Here, we have replaced the momentum sum with an energy integral as  $\sum_{\mathbf{k}}(\dots) \simeq D(\epsilon_F) \int d\epsilon(\dots)$ . Similarly, the reverse process, in which a spin- $\uparrow$  electron transfers from the dot into the left lead, occurs at the rate

$$\Gamma_{(\uparrow,m) \rightarrow (0,m)} = \Gamma_L \left[ 1 - f_L \left( \epsilon_d + \frac{\hbar}{2} \right) \right]. \quad (27)$$

The tunneling rates involving the right lead and the spin- $\downarrow$  state are obtained in a manner analogous to that of the left lead.

$$\Gamma_{(0,m) \rightarrow (\downarrow,m)} = \Gamma_R f_R \left( \epsilon_d - \frac{\hbar}{2} \right), \quad (28)$$

$$\Gamma_{(\downarrow,m) \rightarrow (0,m)} = \Gamma_R \left[ 1 - f_R \left( \epsilon_d - \frac{\hbar}{2} \right) \right]. \quad (29)$$

where  $f_R(\epsilon) = (e^{(\epsilon - \mu_R)/k_B T} + 1)^{-1}$ .

## C. Spin-phonon conversion at a dot

We note that there is no current through a dot solely due to electron transfer from the lead-dot coupling. To obtain a finite current, a spin-flip process at the dot is required. The spin flipping process due to the spin-rotation coupling  $H_{\text{SR}}$  involves phonon absorptions and emissions. Based on Fermi's golden rule, the transition rate from  $(\uparrow, m)$  to  $(\downarrow, m+1)$  is calculated as

$$\Gamma_{(\uparrow,m) \rightarrow (\downarrow,m+1)} = \Gamma_{\text{SR}}^+(m+1), \quad (30)$$

$$\Gamma_{(\downarrow,m+1) \rightarrow (\uparrow,m)} = \Gamma_{\text{SR}}^-(m+1), \quad (31)$$

where  $\Gamma_{\text{SR}}^{\pm} = A\delta(h \mp \hbar\omega_0)$  and  $A$  is given by

$$\begin{aligned} A &= \frac{2\hbar^2\omega_0}{\pi R^2 L \rho} \sin^2 \varphi \\ &= \frac{2\hbar^2\omega_0^2}{\pi^2 R^2} \sqrt{\frac{1}{GS\rho}} \sin^2 \varphi. \end{aligned} \quad (32)$$

For actual calculations, we replace the delta function with a Lorentzian function as [42–44]

$$\delta(h \mp \hbar\omega_0) \rightarrow \frac{\hbar\Gamma/2\pi}{(h \mp \hbar\omega_0)^2 + (\hbar\Gamma/2)^2} \quad (33)$$

with a broadening factor  $\Gamma$ , which is induced by both energy relaxation and electron transfer between the leads and the dot. In the following calculation, we always set the parameters to satisfy  $\Gamma_L, \Gamma_R \gg k_{\text{relax}}$ , for which the choice of  $\Gamma = \Gamma_L + \Gamma_R$  is suitable. To characterize the strength of the spin-rotation coupling, we define the spin-flipping rate on the resonance as

$$\Gamma_{\text{SR}} \equiv \Gamma_{\text{SR}}^{\pm} \Big|_{h=\pm\hbar\omega_0} = \frac{4\hbar\omega_0^2}{\pi^3 \Gamma R^2} \sqrt{\frac{1}{GS\rho}} \sin^2 \varphi. \quad (34)$$

The spin-rotation coupling is enhanced for a small broadening factor  $\Gamma$ , a small radius  $R$ , and a large resonant frequency  $\omega_0$ .

## D. Master equation

To evaluate transport properties, we derive a master equation for the probabilities  $P_{\alpha,m}$  of staying at a joint electron-phonon state  $(\alpha, m)$ , incorporating the transition rates derived above. The master equation is given as

$$\begin{aligned} \dot{P}_{0,m} &= -\Gamma_L f_L P_{0,m} + \Gamma_L (1 - f_L) P_{\uparrow,m} \\ &\quad + \Gamma_R (1 - f_R) P_{\downarrow,m} - \Gamma_R f_R P_{0,m} + \mathcal{D}[P_{0,m}], \end{aligned} \quad (35)$$

$$\begin{aligned} \dot{P}_{\uparrow,m} &= -\Gamma_{\text{SR}}^+(m+1) P_{\uparrow,m} + \Gamma_{\text{SR}}^-(m+1) P_{\downarrow,m+1} \\ &\quad + \Gamma_L f_L P_{0,m} - \Gamma_L (1 - f_L) P_{\uparrow,m} + \mathcal{D}[P_{\uparrow,m}], \end{aligned} \quad (36)$$

$$\begin{aligned} \dot{P}_{\downarrow,m} &= \Gamma_{\text{SR}}^-(m+1) P_{\downarrow,m+1} - \Gamma_{\text{SR}}^+(m+1) P_{\downarrow,m} \\ &\quad - \Gamma_R (1 - f_R) P_{\downarrow,m} + \Gamma_R f_R P_{0,m} + \mathcal{D}[P_{\downarrow,m}], \end{aligned} \quad (37)$$

$$\begin{aligned} \mathcal{D}[P_{\alpha,m}] &= k_{\text{relax}} [m(1 + f_{\text{BE}}) P_{\alpha,m-1} - (m+1) f_{\text{BE}} P_{\alpha,m} \\ &\quad + (m+1) f_{\text{BE}} P_{\alpha,m+1} - m(1 + f_{\text{BE}}) P_{\alpha,m}]. \end{aligned} \quad (38)$$

The steady-state probability distribution is obtained by setting  $\dot{P}_{0,m} = \dot{P}_{\uparrow,m} = \dot{P}_{\downarrow,m} = 0$  under the condition  $\sum_{\alpha,m} P_{\alpha,m} = 1$ . In actual calculation, we take a large cutoff  $m_{\text{max}}$  and consider the probability distribution  $P_{\alpha,m}$  in a finite range of  $0 \leq m \leq m_{\text{max}}$ .

The steady-state current from the dot to the left lead is calculated from the probability distribution as

$$I = e\Gamma_L \sum_m [f_L P_{0,m} + (1 - f_L) P_{\uparrow,m}], \quad (39)$$

where  $e (> 0)$  is the elementary charge.

## E. Phonon driving

In our setup, when a source-drain bias is applied to two half-metallic electrodes in an antiparallel configuration, only a spin- $\uparrow$  electron can enter the quantum dot from the left electrode, while a spin- $\downarrow$  electron can leave

it into the right electrode. In the absence of spin flipping in the quantum dot, no current flows due to the spin valve effect. Spin-flip transitions due to the SRC become effective when the resonance condition  $\hbar\omega_0 \approx h$  is satisfied, enabling a resonant mechanism for spin-phonon conversion. This phonon driving can be detected in the charge current through the CNT.

To see the feasibility of the proposed scheme for driving the torsional vibration of the CNT, we roughly estimate the experimental conditions. We consider a single-wall CNT with a radius  $R \approx 0.5$  nm, a wall thickness  $d \approx 0.34$  nm, and a length  $L = 100$  nm. The cross-sectional area  $S = 2\pi R d \approx 1.1 \times 10^{-18}$  m<sup>2</sup> and the linear mass density  $\rho \approx 2.4 \times 10^{-15}$  kg/m are calculated from the surface density of graphene  $7.6 \times 10^{-7}$  kg/m<sup>2</sup>. The shear modulus  $G$  is taken as 0.41 TPa, based on theoretical calculations and experimental reports [45, 46]. Substituting into the dispersion relation for torsional waves, we find the lowest eigenfrequency of the CNT to be  $\omega_0 \approx 4.3 \times 10^{11}$  rad/s. These frequencies correspond to the phonon energy on the order of  $\hbar\omega_0 \sim 280$   $\mu$ eV, which is comparable to the Zeeman splitting at magnetic fields of 2.4 T. By choosing  $\hbar\Gamma_L = \hbar\Gamma_R = 2.0$   $\mu$ eV, the spin flipping rate at the resonance condition  $h = \hbar\omega_0$  is roughly estimated as  $\hbar\Gamma_{SR} \simeq 1.7 \times 10^{-2}$   $\mu$ eV, which is comparable to the phonon relaxation rate  $k_{\text{relax}}$ . This estimate indicates that driving the torsional vibration of the CNT is experimentally feasible under realistic conditions, utilizing efficient spin-phonon conversion at the resonance condition  $h = \hbar\omega_0$ .

#### IV. RESULT

In this section, we present numerical results for the steady-state probability distribution and the corresponding current. For simplicity, we set the center of the energy levels as  $\epsilon_d = 0$  in the following. Through this section, the shear modulus, the radius of the CNT, the tilting angle, and the tunneling rates are taken as  $G = 0.41$  TPa,  $R = 0.5$  nm,  $\varphi = \pi/4$ , and  $\hbar\Gamma_L = \hbar\Gamma_R = 2.0$   $\mu$ eV, respectively.

##### A. Resonant behavior

Figure 3 shows the steady-state current as a function of the Zeeman splitting energy  $h$  and the phonon energy  $\hbar\omega_0$ , where the phonon frequency  $\omega_0$  is controlled by the CNT length  $L$ . We set the center of the energy levels as  $\epsilon_d = 0$  and the chemical potentials as  $\mu_L = -\mu_R = 150$   $\mu$ eV, for which the energy levels of the CNT,  $\epsilon_\uparrow = h/2$  and  $\epsilon_\downarrow = -h/2$ , are in the energy window  $[\mu_R, \mu_L]$ , allowing electron transfer between the dot and the two leads when  $h < 300$   $\mu$ eV. The other parameters are given in the caption of Fig. 3. The most prominent feature in the figure is a sharp ridge appearing along the

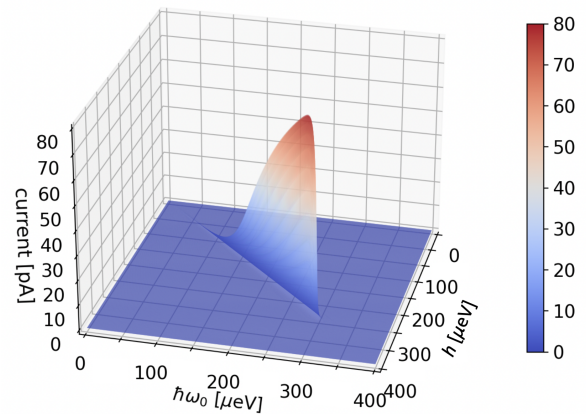


FIG. 3. Contour plot of the current as a function of  $\hbar\omega_0$  and  $h$ . The parameters are set as  $k_B T = 2.0$   $\mu$ eV = 23.2 mK,  $\mu_L = -\mu_R = 150$   $\mu$ eV, and  $k_{\text{relax}} = 3.0 \times 10^{-5} \omega_0$ .

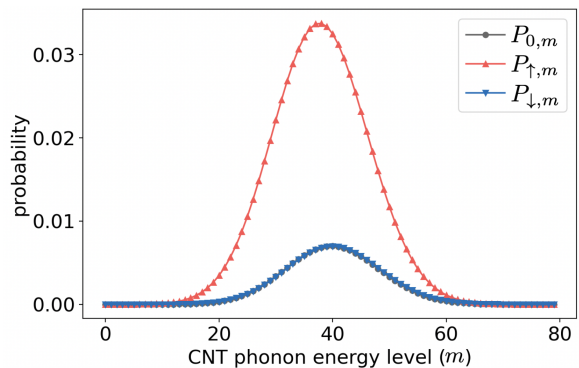


FIG. 4. Probability distributions of the CNT torsional mode. The parameters are set as  $h = \hbar\omega_0 = 250$   $\mu$ eV,  $k_B T = 2.0$   $\mu$ eV = 23.2 mK,  $\mu_L = -\mu_R = 150$   $\mu$ eV, and  $k_{\text{relax}} = 3.0 \times 10^{-5} \omega_0$ .

diagonal line  $h = \hbar\omega_0$ , on which the energy difference between the spin- $\uparrow$  and spin- $\downarrow$  states matches the phonon energy. Under this resonant condition, the spin-rotation coupling efficiently facilitates spin-flip transitions accompanied by phonon emission, bridging the two spin states and allowing a continuous flow of electrons from the left lead to the right lead. The current reaches a maximum order of approximately 80 pA, which is sufficiently detectable in experiments.

##### B. Phonon populations

Figure 4 shows the probability distributions  $P_{\alpha,m}$  under the resonance condition  $h = \hbar\omega_0$ . One finds that  $P_{\uparrow,m}$  shows an excess over  $P_{0,m}$  and  $P_{\downarrow,m}$ , indicating the successful driving of the torsional mode of the CNT. The average phonon population depends on the ratio between the spin flipping rate and the phonon relaxation rate because the steady state is achieved by a balance between

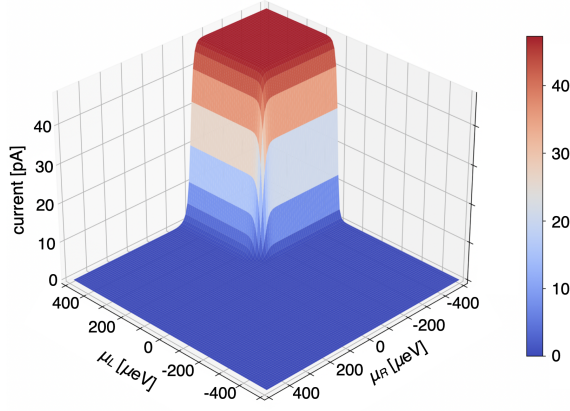


FIG. 5. Contour plot of the current as a function of  $\mu_L$  and  $\mu_R$ . The parameters are set as  $h = \hbar\omega_0 = 200 \mu\text{eV}$ ,  $k_B T = 10.0 \mu\text{eV} = 116 \text{mK}$ , and  $k_{\text{relax}} = 3.0 \times 10^{-5} \omega_0$ .

these two processes. We will discuss this feature in detail in Sec. IV D. The phonon populations show the relation  $P_{\uparrow,m} > P_{0,m} \simeq P_{\downarrow,m}$ , reflecting that the bottleneck of electron transfer through the dot arises from spin flipping due to spin-rotation coupling.

Using this result, we estimate the order of magnitude of the torsional displacement amplitude in the CNT. According to Eqs. (10) and (11), the amplitude operator for the fundamental torsional mode,  $\hat{\theta}$ , is given by

$$\hat{\theta} = \sqrt{\frac{\hbar}{2\rho R^2 \omega_0}} (\hat{a} + \hat{a}^\dagger). \quad (40)$$

Based on the quantization scheme given in Eq. (12), the amplitude of the torsional angle at the center of the CNT is estimated as

$$\mathcal{O}(\theta) \approx \sqrt{\frac{2}{L} \langle \hat{\theta}^2 \rangle} = \frac{1}{R} \sqrt{\frac{\hbar}{\pi} \sqrt{\frac{1}{\rho G S}} (2\langle m \rangle + 1)}. \quad (41)$$

For  $\langle m \rangle \approx 40$ , we find that  $\mathcal{O}(\theta)$  is approximately 1.1 degrees.

### C. Bias dependence

Figure 5 shows a contour plot of the current as a function of  $\mu_L$  and  $\mu_R$  for  $h = \hbar\omega_0$ . As already mentioned, the current flows when the energies of the two quantum levels,  $\epsilon_\uparrow = h/2$  and  $\epsilon_\downarrow = -h/2$ , are within the bias window  $[\mu_R, \mu_L]$  (see also Fig. 2). This expectation can be verified by Figure 5, which shows that the current flows when both  $\mu_L > h/2$  and  $\mu_R < -h/2$  are satisfied. Once this condition is well fulfilled, the current saturates around 50 pA in the present parameter set. The transition width from the zero-current state to the current saturation is determined by the temperature  $k_B T$ .

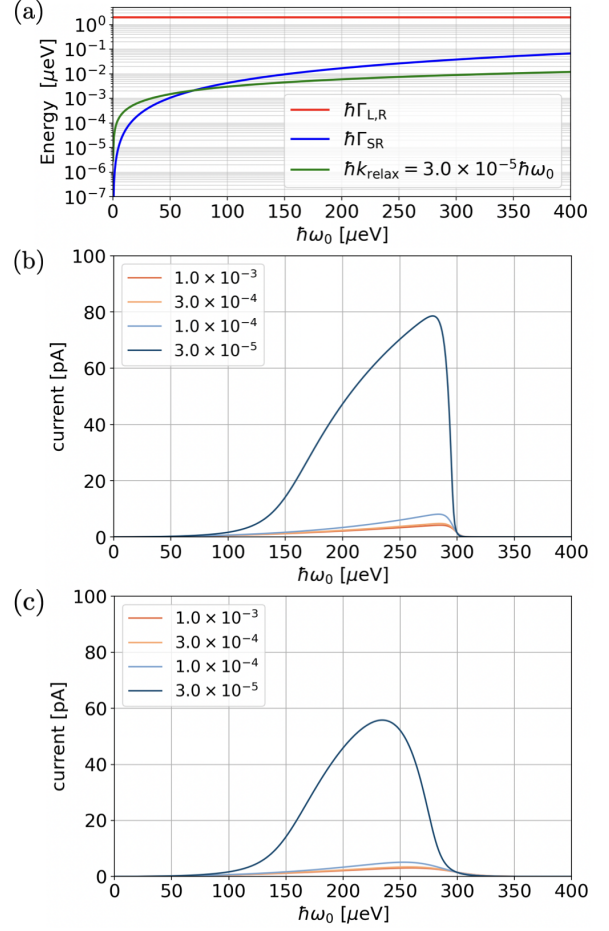


FIG. 6. (a) Comparison of the energy scales for  $\hbar\Gamma_{L,R}$ ,  $\hbar\Gamma_{SR}$  and  $\hbar k_{\text{relax}}$  as a function of  $\hbar\omega_0$ . The damping rate is set as  $k_{\text{relax}} = 3.0 \times 10^{-5} \omega_0$ . Current under the resonant condition ( $h = \hbar\omega_0$ ) is plotted as a function of  $\hbar\omega_0$  at (b)  $k_B T = 2.0 \mu\text{eV} = 23.2 \text{mK}$  and (c)  $k_B T = 10.0 \mu\text{eV} = 116 \text{mK}$ . The other parameters are set as  $h = \hbar\omega_0$ ,  $\mu_L = -\mu_R = 150.0 \mu\text{eV}$ .

### D. Other parameter dependences

Figure 6(a) shows the tunneling rate  $\Gamma_{L,R}$  ( $= \Gamma_L = \Gamma_R$ ), the relaxation rate  $k_{\text{relax}}$ , and the spin-phonon conversion rate  $\Gamma_{SR}$  as functions of the phonon energy  $\hbar\omega_0$ . Within the plotted range of  $\hbar\omega_0$ ,  $\Gamma_{L,R}$  is always much larger than  $\Gamma_{SR}$  and  $k_{\text{relax}}$ . At low phonon frequencies, the phonon damping  $k_{\text{relax}}$  exceeds the spin-flip rate  $\Gamma_{SR}$ , leading to a strong suppression of phonon driving. On the other hand,  $\Gamma_{SR}$  becomes larger than  $k_{\text{relax}}$  for  $\hbar\omega_0 > 70 \mu\text{eV}$ , allowing efficient phonon driving.

Figure 6(b) shows the current as a function of  $\hbar\omega_0$  at  $k_B T = 2.0 \mu\text{eV} = 23.2 \text{mK}$  under the resonant condition  $h = \hbar\omega_0$ . The other parameters are given in the caption of Fig. 6. The four curves correspond to  $k_{\text{relax}}/\omega_0 = 3 \times 10^{-5}$ ,  $1 \times 10^{-4}$ ,  $3 \times 10^{-4}$ , and  $1 \times 10^{-3}$ , respectively. We note that  $k_{\text{relax}}$  is approximately the inverse of the quality factor of the CNT torsional mode. In the low-frequency region ( $\hbar\omega_0 < 70 \mu\text{eV}$ ), the cur-

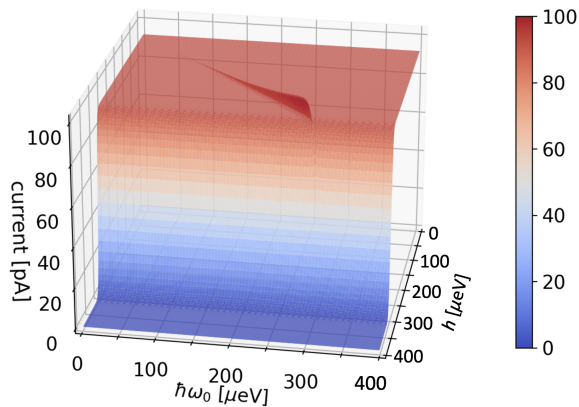


FIG. 7. Contour plot of the current as a function of  $\hbar\omega_0$  and  $h$  for a finite spin polarization  $P = 0.4$ . The parameters are set as  $\hbar\bar{\Gamma}_L = \hbar\bar{\Gamma}_R = 1.0 \mu\text{eV}$  and all other parameters are the same as in Fig. 3.

rent is suppressed by strong phonon damping (see also Fig. 6(a)). In the moderate-frequency region ( $70 \mu\text{eV} < \hbar\omega_0 < 300 \mu\text{eV}$ ), spin-flip processes due to the SRC exceed the phonon damping, leading to a remarkable increase in the current. We note that  $\Gamma_{\text{SR}}$  is proportional to  $\omega_0^2$  according to Eq. (32). In the high-frequency region ( $\hbar\omega_0 > 300 \mu\text{eV}$ ), the current drops again because the energies of the dot levels go outside the bias window  $[\mu_R, \mu_L]$ .

Figure 6(c) shows the frequency dependence of the current at a higher temperature  $k_B T = 10.0 \mu\text{eV} = 116 \text{ mK}$ . Although the overall features are similar to the low-temperature result in Fig. 6(b), the current is reduced. This reduction originates from the thermal broadening of the Fermi-Dirac distribution in the electrodes, as indicated by Eqs. (26)-(29).

## V. DISCUSSION

### A. Realistic ferromagnetic electrodes

Throughout the preceding sections, we have assumed half-metallic electrodes with perfect spin polarization for simplicity. However, for experimental realization it is preferable to use ferromagnetic metals with partial spin polarization, such as Fe, Co, Ni, or their alloys. Our formulation can be extended to such partially polarized electrodes by modifying the transition probabilities between the electrodes and the quantum dot as

$$\Gamma_{(0,m) \rightarrow (\sigma,m)} = \bar{\Gamma}_L (1 + \sigma P) f_L \left( \epsilon_d + \sigma \frac{\hbar}{2} \right) + \bar{\Gamma}_R (1 - \sigma P) f_R \left( \epsilon_d + \sigma \frac{\hbar}{2} \right), \quad (42)$$

where  $P$  is the spin polarization of the electrodes at the Fermi level, and  $\bar{\Gamma}_{L,R}$  are the averaged transition prob-

abilities per spin. The transition probabilities for the inverse processes are obtained by replacing  $f_{R,L}$  with  $1 - f_{R,L}$ . Fig. 7 shows the current as a function of the Zeeman splitting energy  $h$  and the phonon energy  $\hbar\omega_0$  for  $P = 0.4$ . In contrast to the half-metallic electrodes, the current remains finite even away from the resonance. Nevertheless, the SRC-induced resonance remains a robust and experimentally distinguishable feature, as shown in Fig. 7, indicating that our results remain qualitatively valid for a broad class of ferromagnetic contacts.

### B. Spin-Orbit Interaction

In our work, we employ a simplified model for the CNTs. However, in actual CNT systems, the valley degree of freedom and spin-orbit interaction (SOI) cannot be neglected. In the absence of the magnetic field, the SOI lifts the four-fold degeneracy due to the spin and valley degrees of freedom and lowers the energy of  $(K, \uparrow)$  and  $(K', \downarrow)$  relative to  $(K, \downarrow)$  and  $(K', \uparrow)$ , where  $K$  and  $K'$  denote the valley indices. The external magnetic field induces Zeeman splitting of both the spin and orbital angular momenta, the latter of which differs between  $K$  and  $K'$ . Thus, the energy spectrum in real CNTs becomes more complex than our simple model [47–49]. However, by tuning the magnetic field, the energy difference between the two spin states,  $(K, \uparrow)$  and  $(K, \downarrow)$  (or  $(K', \uparrow)$  and  $(K', \downarrow)$ ) can be controlled to match the phonon energy  $\hbar\omega_0$ . Therefore, our simple model is still effective if the magnetic field  $h$  is regarded as a control parameter to change the energy difference between the two spin states.

## VI. SUMMARY

In summary, we theoretically presented a novel mechanism for the current-induced mechanical excitation in carbon nanotube (CNT) quantum dots via spin-rotation coupling. Our analysis, based on a master-equation approach, shows that when the Zeeman splitting matches the eigenfrequency of the CNT torsional mode ( $h = \hbar\omega_0$ ), its amplitude is strongly enhanced through resonant pumping. Importantly, this mechanism lifts the spin valve effect intrinsic to the antiparallel electrode configuration, giving rise to a measurable leakage current to flow in a regime where transport would otherwise be suppressed.

Numerical estimates for realistic CNT parameters predict a detectable torsional displacement and a current signal on the order of several tens of pA. These signals are well within the sensitivity limits of state-of-the-art nanoelectromechanical measurement techniques. Furthermore, we have confirmed that the mechanism remains robust even in the presence of complex energy spectra due to realistic SOI in CNTs, provided the magnetic field is used as a control parameter.

Our findings establish a purely electronic scheme for the control of mechanical rotational oscillation and offer a promising platform for the development of next-generation spin-driven mechanical systems.

### ACKNOWLEDGMENTS

This work was supported by the Priority Program of Chinese Academy of Sciences under Grant No. XDB28000000, and by JSPS KAKENHI for Grants (JP24K06951) from MEXT, Japan.

### Appendix A: Hamiltonian formalism of torsional oscillations

In this Appendix, we present a detailed derivation of the quantized torsional modes of a CNT. Within the continuum approximation, the torsional displacement  $\theta(z)$  is conjugate to the angular-momentum density  $\pi(z)$ , and the classical Hamiltonian describing the system is given by

$$H = \int_0^L dz \left[ \frac{1}{2\rho R^2} \pi^2(z) + \frac{GSR^2}{2} (\partial_z \theta(z))^2 \right], \quad (\text{A1})$$

where  $\rho$  is the mass density per unit length,  $R$  is the radius,  $G$  is the shear modulus, and  $S = 2\pi R d$  is the cross-sectional area. For simplicity, we have replaced  $z'$  with  $z$ . The canonical equations of motion are

$$\dot{\theta}(z, t) = \frac{\delta H}{\delta \pi(z, t)} = \frac{\pi(z, t)}{\rho R^2}, \quad (\text{A2})$$

$$\dot{\pi}(z, t) = -\frac{\delta H}{\delta \theta(z, t)} = GSR^2 \partial_z^2 \theta(z, t), \quad (\text{A3})$$

leading to the wave equation, Eq. (7).

To quantize the system, we impose the canonical commutation relation  $[\hat{\theta}(z), \hat{\pi}(z')] = i\hbar\delta(z - z')$ . Under the boundary conditions  $\theta(0, t) = \theta(L, t) = 0$ , we expand the

field operators in terms of normal modes as

$$\hat{\theta}(z) = \sum_{n=1}^{\infty} \sqrt{\frac{2}{L}} \sin(k_n z) \hat{\theta}_n, \quad (\text{A4})$$

$$\hat{\pi}(z) = \sum_{n=1}^{\infty} \sqrt{\frac{2}{L}} \sin(k_n z) \hat{\pi}_n, \quad (\text{A5})$$

where  $k_n = n\pi/L$ . The mode operators satisfy the discrete commutation relation  $[\hat{\theta}_n, \hat{\pi}_{n'}] = i\hbar\delta_{nn'}$ . Substituting these expansions into Eq. (A1) and utilizing the orthogonality of the sine functions, the Hamiltonian is diagonalized as

$$H = \sum_{n=1}^{\infty} \left[ \frac{1}{2\rho R^2} \hat{\pi}_n^2 + \frac{\rho R^2 \omega_n^2}{2} \hat{\theta}_n^2 \right], \quad (\text{A6})$$

where  $\omega_n = ck_n$  is the eigenfrequency of the  $n$ -th mode.

Next, we introduce the bosonic annihilation and creation operators  $\hat{a}_n^\dagger$  and  $\hat{a}_n$ :

$$\hat{a}_n = \sqrt{\frac{\rho R^2 \omega_n}{2\hbar}} \left( \hat{\theta}_n + i \frac{\hat{\pi}_n}{\rho R^2 \omega_n} \right), \quad (\text{A7})$$

$$\hat{a}_n^\dagger = \sqrt{\frac{\rho R^2 \omega_n}{2\hbar}} \left( \hat{\theta}_n - i \frac{\hat{\pi}_n}{\rho R^2 \omega_n} \right). \quad (\text{A8})$$

These operators satisfy  $[\hat{a}_n, \hat{a}_{n'}^\dagger] = \delta_{nn'}$ , and the Hamiltonian takes the standard second-quantized form  $H = \sum_n \hbar\omega_n (\hat{a}_n^\dagger \hat{a}_n + 1/2)$ . In the Heisenberg picture, the time-dependent torsional operator for the fundamental mode ( $n = 1$ ) is expressed as

$$\hat{\theta}_1(t) = \sqrt{\frac{\hbar}{2\rho R^2 \omega_1}} (\hat{a}_1 e^{-i\omega_1 t} + \hat{a}_1^\dagger e^{i\omega_1 t}), \quad (\text{A9})$$

$$\hat{\pi}_1(t) = -i\sqrt{\frac{\hbar\rho R^2 \omega_1}{2}} (\hat{a}_1 e^{-i\omega_1 t} - \hat{a}_1^\dagger e^{i\omega_1 t}). \quad (\text{A10})$$

The former equation corresponds to the time evolution of the operator  $\hat{\theta}$  given in Eq. (13) of the main text.

- 
- [1] H. G. Craighead, Nanoelectromechanical systems, *Science* **290**, 1532 (2000).
- [2] S. Saplaz, Y. M. Blanter, L. Gurevich, and H. S. J. Van der Zant, Carbon nanotubes as nanoelectromechanical systems, *Phys. Rev. B* **67**, 235414 (2003).
- [3] V. Sazonova, Y. Yaish, H. Üstünel, D. Roundy, T. A. Arias, and P. L. McEuen, A tunable carbon nanotube electromechanical oscillator, *Nature* **431**, 284 (2004).
- [4] M. Poot and H. S. J. van der Zant, Mechanical systems in the quantum regime, *Physics Reports* **511**, 273 (2012).
- [5] B. Xu, P. Zhang, J. Zhu, Z. Liu, A. Eichler, X.-Q. Zheng, J. Lee, A. Dash, S. More, S. Wu, Y. Wang, H. Jia, A. Naik, A. Bachtold, R. Yang, P. X. L. Feng, and Z. Wang, Nanomechanical resonators: Toward atomic scale, *ACS Nano* **16**, 15545 (2022).
- [6] S. J. Papadakis, A. R. Hall, P. A. Williams, L. Vicci, M. R. Falvo, R. Superfine, and S. Washburn, Resonant Oscillators with Carbon-Nanotube Torsion Springs, *Phys. Rev. Lett.* **93**, 146101 (2004).
- [7] A. R. Hall, M. R. Falvo, R. Superfine, and S. Washburn, A Self-Sensing Nanomechanical Resonator Built on a Single-Walled Carbon Nanotube, *Nano Lett.* **8**, 3746 (2008).
- [8] K. Mori, M. G. Dunsmore, J. E. Losby, D. M. Jenson, M. Belov, and M. R. Freeman, Einstein-de Haas effect at radio frequencies in and near magnetic equilibrium, *Phys. Rev. B* **102**, 054415 (2020).
- [9] A. K. Hüttel, G. A. Steele, B. Witkamp, M. Poot,

- L. P. Kouwenhoven, and H. S. van der Zant, Carbon Nanotubes as Ultrahigh Quality Factor Mechanical Resonators, *Nano Lett.* **9**, 2547 (2009).
- [10] G. A. Steele, A. K. Hüttel, B. Witkamp, M. Poot, H. B. Meerwaldt, L. P. Kouwenhoven, and H. S. van der Zant, Strong Coupling Between Single-Electron Tunneling and Nanomechanical Motion, *Science* **325**, 1103 (2009).
- [11] B. Lassagne, Y. Tarakanov, J. Kinaret, D. Garcia-Sanchez, and A. Bachtold, Coupling Mechanics to Charge Transport in Carbon Nanotube Mechanical Resonators, *Science* **325**, 1107 (2009).
- [12] E. A. Laird, F. Kuemmeth, G. A. Steele, K. Grove-Rasmussen, J. Nygård, K. Flensberg, and L. P. Kouwenhoven, Quantum transport in carbon nanotubes, *Rev. Mod. Phys.* **87**, 703 (2015).
- [13] W. Izumida, R. Okuyama, and R. Saito, Valley coupling in finite-length metallic single-wall carbon nanotubes, *Phys. Rev. B* **91**, 235442 (2015).
- [14] W. Izumida, R. Okuyama, A. Yamakage, and R. Saito, Angular momentum and topology in semiconducting single-wall carbon nanotubes, *Phys. Rev. B* **93**, 195442 (2016).
- [15] K. L. Ekinci and M. L. Roukes, Nanoelectromechanical systems, *Rev. Sci. Instrum.* **76**, 061101 (2005).
- [16] S. J. Barnett, Magnetization by Rotation, *Phys. Rev.* **6**, 239 (1915).
- [17] A. Einstein and W. J. de Haas, Experimental proof of the existence of ampère's molecular currents, *KNAW proc.* **18 I**, 696 (1915).
- [18] S. J. Barnett, Gyromagnetic and Electron-Inertia Effects, *Rev. Mod. Phys.* **7**, 129 (1935).
- [19] G. G. Scott, Review of Gyromagnetic Ratio Experiments, *Rev. Mod. Phys.* **34**, 102 (1962).
- [20] M. Matsuo, J. Ieda, K. Harii, E. Saitoh, and S. Maekawa, Mechanical generation of spin current by spin-rotation coupling, *Phys. Rev. B* **87**, 180402 (2013).
- [21] M. Matsuo, Y. Ohnuma, and S. Maekawa, Theory of spin hydrodynamic generation, *Phys. Rev. B* **96**, 020401 (2017).
- [22] M. Matsuo, E. Saitoh, and S. Maekawa, Spin-Mechatronics, *J. Phys. Soc. Jpn.* **86**, 011011 (2017).
- [23] R. Takahashi, M. Matsuo, M. Ono, K. Harii, H. Chudo, S. Okayasu, J. Ieda, S. Takahashi, S. Maekawa, and E. Saitoh, Spin hydrodynamic generation, *Nat. Phys.* **12**, 52 (2016).
- [24] R. Takahashi, H. Chudo, M. Matsuo, K. Harii, Y. Ohnuma, S. Maekawa, and E. Saitoh, Giant spin hydrodynamic generation in laminar flow, *Nat. Commun.* **11**, 3009 (2020).
- [25] H. Tabaei Kazerooni, A. Thieme, J. Schumacher, and C. Cierpka, Electron spin-vorticity coupling in pipe flows at low and high Reynolds number, *Phys. Rev. Appl.* **14**, 014002 (2020).
- [26] H. Tabaei Kazerooni, G. Zinchenko, J. Schumacher, and C. Cierpka, Electrical voltage by electron spin-vorticity coupling in laminar ducts, *Phys. Rev. Fluids* **6**, 043703 (2021).
- [27] D. Kobayashi, T. Yoshikawa, M. Matsuo, R. Iguchi, S. Maekawa, E. Saitoh, and Y. Nozaki, Spin Current Generation Using a Surface Acoustic Wave Generated via Spin-Rotation Coupling, *Phys. Rev. Lett.* **119**, 077202 (2017).
- [28] Y. Kurimune, M. Matsuo, and Y. Nozaki, Observation of Gyromagnetic Spin Wave Resonance in NiFe Films, *Phys. Rev. Lett.* **124**, 217205 (2020).
- [29] Y. Kurimune, M. Matsuo, S. Maekawa, and Y. Nozaki, Highly nonlinear frequency-dependent spin-wave resonance excited via spin-vorticity coupling, *Phys. Rev. B* **102**, 174413 (2020).
- [30] S. Tateno, Y. Kurimune, M. Matsuo, K. Yamanoi, and Y. Nozaki, Einstein–de Haas phase shifts in surface acoustic waves, *Phys. Rev. B* **104**, L020404 (2021).
- [31] T. Funato, S. Kinoshita, N. Tanahashi, S. Nakamura, and M. Matsuo, Spin current generation due to differential rotation, *Phys. Rev. B* **111**, L060403 (2025).
- [32] A. N. Cleland, *Foundations of Nanomechanics: From Solid-State Theory to Device Applications* (Springer, Berlin, Germany, 2003).
- [33] P. Mohanty, G. Zolfagharkhani, S. Kettemann, and P. Fulde, Spin-mechanical device for detection and control of spin current by nanomechanical torque, *Phys. Rev. B* **70**, 195301 (2004).
- [34] T. M. Wallis, J. Moreland, and P. Kabos, Einstein–de Haas effect in a NiFe film deposited on a microcantilever, *Appl. Phys. Lett.* **89**, 122502 (2006).
- [35] G. Zolfagharkhani, A. Gaidarzhly, P. Degiovanni, S. Kettemann, P. Fulde, and P. Mohanty, Nanomechanical detection of itinerant electron spin flip, *Nat. Nanotechnol.* **3**, 720 (2008).
- [36] K. Harii, Y.-J. Seo, Y. Tsutsumi, H. Chudo, K. Oyanagi, M. Matsuo, Y. Shiomi, T. Ono, S. Maekawa, and E. Saitoh, Spin Seebeck mechanical force, *Nat. Commun.* **10**, 2616 (2019).
- [37] F. W. Hehl and W.-T. Ni, Inertial effects of a Dirac particle, *Phys. Rev. D* **42**, 2045 (1990).
- [38] M. Matsuo, J. Ieda, E. Saitoh, and S. Maekawa, Effects of Mechanical Rotation on Spin Currents, *Phys. Rev. Lett.* **106**, 076601 (2011).
- [39] H. Suzuura and T. Ando, Phonons and electron-phonon scattering in carbon nanotubes, *Phys. Rev. B* **65**, 235412 (2002).
- [40] M. Hamada, E. Minamitani, M. Hirayama, and S. Murakami, Phonon angular momentum induced by the temperature gradient, *Phys. Rev. Lett.* **121**, 175301 (2018).
- [41] W. Izumida, R. Okuyama, K. Sato, T. Kato, and M. Matsuo, Einstein–de Haas Nanorotor, *Phys. Rev. Lett.* **128**, 017701 (2022).
- [42] H. Schoeller and G. Schön, Mesoscopic quantum transport: Resonant tunneling in the presence of a strong Coulomb interaction, *Phys. Rev. B* **50**, 18436 (1994).
- [43] C. Timm, Tunneling through molecules and quantum dots: Master-equation approaches, *Phys. Rev. B* **77**, 195416 (2008).
- [44] H. Bruus and K. Flensberg, *Many-Body Quantum Theory in Condensed Matter Physics: An Introduction*, 2nd ed. (Oxford University Press, Oxford, 2016).
- [45] J. P. Lu, Elastic properties of carbon nanotubes and nanoropes, *Phys. Rev. Lett.* **79**, 1297 (1997).
- [46] A. R. Hall, L. An, J. Liu, L. Vicci, M. R. Falvo, R. Superfine, and S. Washburn, Experimental measurement of single-wall carbon nanotube torsional properties, *Phys. Rev. Lett.* **96**, 256102 (2006).
- [47] F. Kuemmeth, S. Ilani, D. C. Ralph, and P. L. McEuen, Coupling of spin and orbital motion of electrons in carbon nanotubes, *Nature* **452**, 448 (2008).
- [48] W. Izumida, K. Sato, and R. Saito, Spin–Orbit Interaction in Single Wall Carbon Nanotubes: Symmetry Adapted Tight-Binding Calculation and Effective Model

Analysis, *J. Phys. Soc. Jpn.* **78**, 074707 (2009).  
[49] J. Klinovaja, M. J. Schmidt, B. Braunecker, and D. Loss,

Carbon nanotubes in electric and magnetic fields, *Phys. Rev. B* **84**, 085452 (2011).